환경영향평가 Vol. 34, No. 5(2025), pp.314-328 J. Environ. Impact Assess. 34(5): 314-328(2025) ISSN 1225-7184
https://doi.org/10.14249/eia.2025.34.5.314

Research Paper

Assessing Mechanisms of Reduced Dispersion in Response to Coastal Development: Comparison of Concentration- and Particle-Derived Diffusion Indices

HyeRyeon Gwon* · JongGu Kim* · Hoon Kang · MinSun Kwon*****

Department of Environmental Engineering, Kunsan National University*
Marine Energy Division, MIT co., Ltd.**
Ocean Physics Dept., Land & Ocean Environmental Eng.***

연안 개발에 따른 물질 확산 저해 메커니즘 분석: 농도·입자 기반 유효확산계수 비교

권혜련* · 김종구 · 강 훈*** · 권민선*****

군산대학교 토목환경공학부*, 군산대학교 환경공학과 교수**,
(주)해양정보기술***, (주)국토해양환경기술단*****

요약: 본 연구는 새만금 신항만 건설에 따른 유로 재편성과 구조물 설치가 해수 유입 및 물질 수송 특성에 미치는 영향을 정량적으로 규명하기 위해 수행되었다. 이를 위해 EFDC 모델을 활용하여 개발 전(2013, Case 0), 부분 개발(2023, Case 1), 완공 후(2030, Case 2) 조건의 3차원 해수유동을 모의하고, 염분 분포, 수직 염분 구배, 유효확산계수(Deff), 입자 이동 특성을 종합적으로 분석하였다. 분석 결과, 동진수역(Box 6)은 동서도로 건설과 수로 정렬로 인해 혼합이 활발해진 반면, 만경수역(Box 5)은 유입 경로가 제한되면서 체류 시간이 증가하는 등 상반된 경향을 보였다. 농도 기반 확산계수는 수로 정렬로 인한 농도 구배 완화와 같은 평균적 혼합 특성을 반영하는 반면, 입자 기반 확산계수는 잔차류에 의한 이송 효과와 국소적 순환 구조의 영향을 나타내어 국지적 물질 이송 특성을 파악하는 데 유효하였다. 따라서 두 확산계수는 서로 다른 측면의 확산 메커니즘을 보여주는 상호보완적 지표로서, 병행 해석을 통해 구조물 설치가 구역별 물질 교환에 미치는 영향을 물리적으로 규명할 수 있었다. 특히 만경수역과 같이 장기 체류가 발생하기 쉬운 구역에서는 체류수 관리 및 수문 운영의 개선이 필요함을 시사하였다.

주요어: 새만금 , EFDC, 유효확산계수, 입자추적, 잔차류

Abstract: This study quantitatively investigated the effects of flow reorganization and structural installations associated with the Saemangeum New Port construction on seawater inflow and material

First Author: HyeRyeon Gwon, Tel: 82-63-469-1871, Email: gwonhr@kunsan.ac.kr, ORCID: 0009-0005-3427-7272
Corresponding Author: MinSun Kwon, Tel: +82-31-695-3474, Email: mskwon@landocean.co.kr, ORCID: 0000-0003-0932-0070
Co-Authors: JongGu Kim, Tel: 82-63-469-1874, Email: kjg466@kunsan.ac.kr, ORCID: 0000-0003-0451-5565
Hoon Kang, Tel: 82-63-469-1871, Email: kh1023@daum.net, ORCID: 0000-0003-0867-5865

Received: 1 October, 2025. Revised: 24 October, 2025. Accepted: 27 October, 2025.

transport characteristics. The EFDC model was applied to simulate three-dimensional hydrodynamics under three scenarios: pre-development (2013, Case 0), partial development (2023, Case 1), and post-completion (2030, Case 2). Comprehensive analyses were conducted on salinity distribution, vertical salinity gradient, effective diffusion coefficient (Deff), and particle transport characteristics. The results revealed contrasting trends between regions: the Dongjin area (Box 6) exhibited enhanced mixing due to the east–west road and channel realignment, whereas the Mangyeong area (Box 5) showed increased residence time owing to restricted inflow pathways. The concentration-based diffusion coefficient represented large-scale mixing processes, reflecting the attenuation of salinity gradients, while the particle-based diffusion coefficient captured the effects of residual currents and local circulation, providing insights into localized material transport. These two diffusion coefficients thus served as complementary indicators, elucidating different aspects of the diffusion mechanism. Their combined interpretation clarified how structural modifications influence material exchange across regions and highlighted the need for improved management of stagnant zones such as the Mangyeong area.

Keywords : Saemangeum, EFDC, Effective diffusion coefficient, Particle Tracking, Residual Current

I. Introduction

The Saemangeum Development Project is a large-scale national project aimed at constructing a 33.9 km seawall from Bieung-dong in Gunsan to Byeonsan-myeon in Buan, thereby creating a total reclaimed area of 291 km² and a freshwater lake of 118 km². Construction commenced in 1991, the closure was completed in 2006, and the seawall was fully constructed in 2010 (Chun, 2003; Park, 2016; Lee, 2008). With the disconnection from the open sea caused by the seawall, the hydrodynamic and water quality characteristics of the Saemangeum Reservoir have since been controlled by river inflows and seawater intrusion through the sluice gates (Jeong et al., 2009). However, stratification due to the density difference between freshwater and seawater has led to the intensification of pollutant retention and sedimentation, resulting in water quality degradation.

To analyze the impacts of seawall construction on water quality and ecosystems in Saemangeum, numerous studies have been conducted (Kim et al., 2002; Ko et al., 2002; Jeong et al., 2018), and considerable efforts have been made to predict hydrodynamic changes caused by structural installation and sluice gate operations. Suh and Cho (2007) reported, through numerical experiments, that after the final closure of the seawall, the inlet width was reduced, tidal volume decreased, tidal asymmetry and flood dominance intensified, and water levels rose within the reservoir. Suh and Lee (2011) applied a particle-tracking model to evaluate stepwise hydrodynamic changes from the initial construction to post-closure. They found that the reciprocating flow between the outer Saemangeum and the Mangyeong–Dongjin estuaries, initially in the east–west direction, shifted to the northeast –southwest after the fourth seawall construction. After completion, seawater in the Byeonsan vicinity and Dongjin River estuary predominantly moved seaward under the influence of sluice gate discharge.

Yoo et al. (2012) simulated the internal hydrodynamics of the Saemangeum Reservoir using EFDC, indicating that stratification developed with separation between surface and bottom layers, which generated sluggish bottom circulation and deteriorated water quality. Using particle-tracking techniques, they further assessed retention characteristics under normal and flood conditions, reporting that dredging increased residence time and some northern Mangyeong areas transformed into stagnant zones after internal development. Cho et al. (2020) conducted particle-

tracking experiments to identify the seasonal influence ranges of sluice discharges on the outer Saemangeum region, and quantified the travel time of discharge water using water age as an indirect indicator. Park et al. (2023) analyzed salinity variation and bottom-water exchange under a scenario where sluice operations increased from once to twice per day. Their results showed a maximum water level increase of 0.7 m, salinity changes ranging from +2.12 psu to −1.94 psu, and a decrease in particle retention from 10.22% to 7.70%, demonstrating enhanced bottom-water exchange.

Previous studies on Saemangeum have primarily focused on water quality, velocity, residence time, and salinity distributions within the reservoir, while relatively few have considered both the inner and outer domains simultaneously. Furthermore, most existing studies on material exchange have been limited to the inner Saemangeum, with some particle-tracking analyses addressing inner–outer exchanges. However, these often adopted oversimplified assumptions such as continuous gate openings, or merely quantified particle displacement and exchange amounts, without reflecting realistic gate operations (Suh and Lee, 2011).

To overcome these limitations, this study conducted numerical simulations that incorporated both realistic sluice gate operations and planned developments of the new port and inner reclamation up to 2030. By integrating Eulerian and Lagrangian-based analytical indicators, this study evaluates material transport and stagnation characteristics, thereby providing fundamental insights for hydrodynamic and water quality management as well as long-term environmental strategy development in the Saemangeum region.

II. Materials and Methods

1. Numerical Model Experiments

1) Model Setup

This study employed the Environmental Fluid Dynamics Code (EFDC), a widely used numerical model for coastal and estuarine applications. The computational domain covered approximately 797 km², encompassing both the inner and outer sea areas of Saemangeum, and was used to simulate seawater circulation, salinity diffusion, and particle transport. To represent the operation of the sluice gates, a variable horizontal grid resolution of 240–300 m was applied around the Sin-si Gate (240 m) and Garyeok Gate (300 m). The grid consisted of 141 cells in the x-direction and 141 in the y-direction, resulting in a total of 9,244 active cells. Vertically, the water column was divided into five sigma layers, each representing 20% of the total depth, dynamically adjusted according to tidal

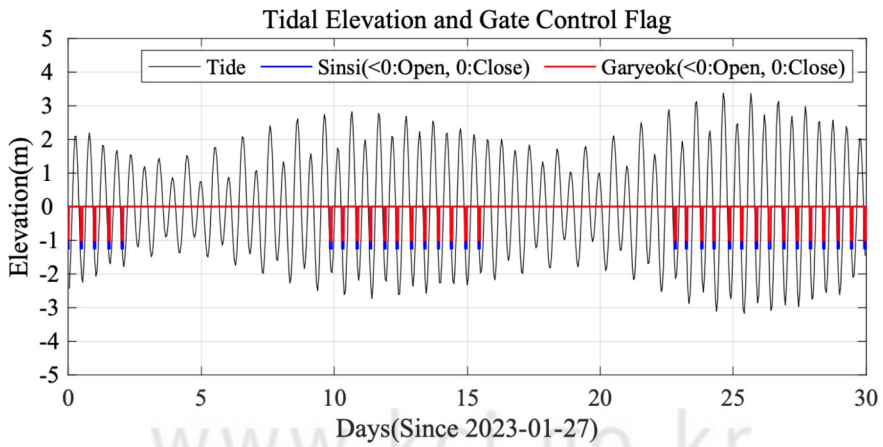

Figure 1. Controlled operation schedule of Saemangeum's tidal sluice gates

variations. The open boundary conditions were specified using tidal elevations calibrated from Gyeogpo Port and Bieung Port, based on data from the Korea Hydrographic and Oceanographic Agency (KHOA). The river inflows were assigned according to the flow rates presented in the Final Report on the Study of Internal Water Quality Characteristics and Management Measures for Saemangeum Lake (2017) — 9.78 m^3/s for the Mangyeong River and 4.38 m^3/s for the Dongjin River.

The simulation period covered 30 days from January 27, 2023, with a time step of 2 seconds. The horizontal diffusion coefficient was set to 1.0 m^2/s, and the vertical diffusion coefficient to 1.0×10^{-6} m^2/s, which appropriately represent momentum diffusion effects. Model verification for currents and tides using these parameters showed good agreement with observations, confirming the model's capability to reproduce the hydrodynamic characteristics of the study area. Sensitivity analysis was not performed,

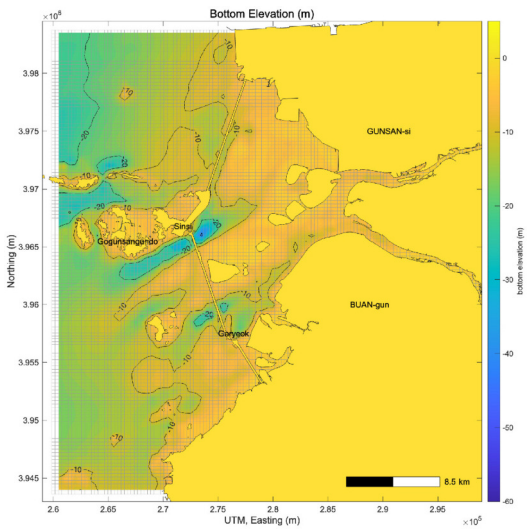

(a) Case 0

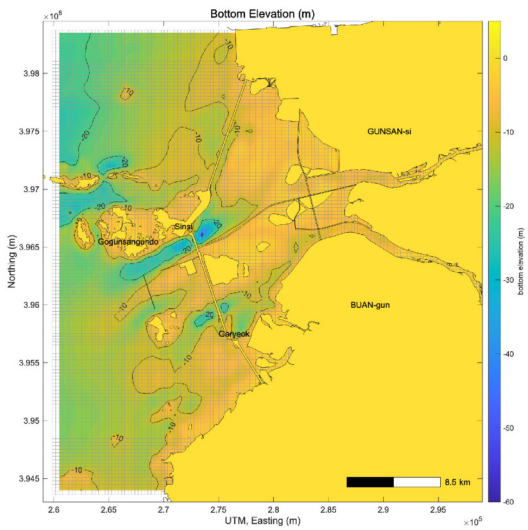

(b) Case 1

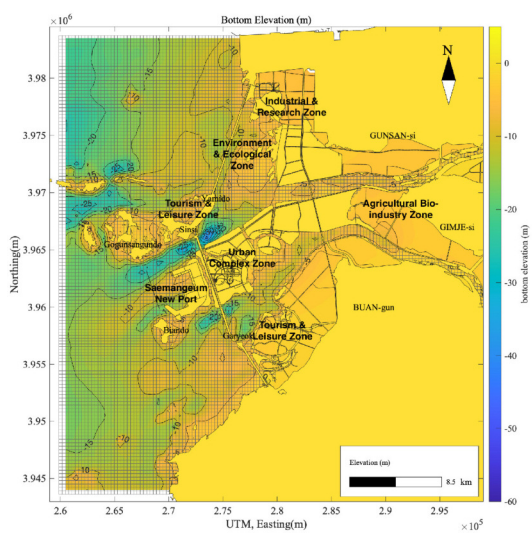

(c) Case 2

Figure 2. EFDC model grid system - Case 0, 1, 2

as it was beyond the scope of this study. To control the opening and closing of the sluice gates, the GATECONTROL subroutine developed by Park et al. (2023) was implemented to represent the actual gate operation cycle according to tidal phases. Bathymetric data were interpolated onto the model grid using 1:5,000-scale bathymetric charts provided by KHOA.

2) Experimental Scenarios

The seawater flow simulations were designed for three development scenarios. Case 0 (Pre-Project, 2013) represented the condition before the construction of the outer breakwater, with partial reclamation of the inner area. Case 1 (Current State, 2023) reflected the completion of the new port's outer breakwater, the East–West and North–South roads, and partial inner reclamation. Case 2 (Post-Project, 2030) assumed the full completion of the new port and all internal reclamation works. The inner reclaimed area is planned as a multi-purpose development zone integrating industrial, port, tourism, agricultural, residential, and ecological functions. It will include an industrial complex and airport in the north, a new port and logistics hub in the west, a tourism and leisure complex in the south, and an agricultural and ecological restoration zone in the center (Fig. 2 (c)). This spatial structure is expected to be a major factor influencing future river channel reorganization as well as hydrological and water quality changes. In all experimental scenarios, salinity was set to 30 psu outside and 0 psu inside the Saemangeum seawall, following observational data from the National Oceanographic Survey Agency, to assess vertical mixing, residence time, and diffusion.

In the particle tracking experiments, a total of 1,000 neutrally buoyant particles were released to ensure statistical robustness. Specifically, 500 particles were released simultaneously at the surface layer (0 m depth) at two freshwater inflow points—the Mangyeong River and Dongjin River—on January 27, 2023, with a tracking duration of 30 days. Particles were advected by three-dimensional tidal currents, with release locations corresponding to actual freshwater inflow zones. Particle motion was computed using the Runge–Kutta integration scheme within the Lagrangian Particle Tracking (LPT) module of EFDC, incorporating random-walk components in both horizontal and vertical directions. The random-walk step size was automatically calculated based on the

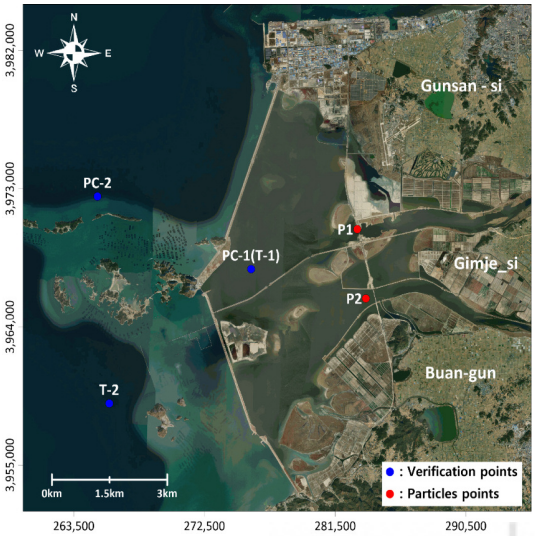

Figure 3. Verification points and initial particles drop points

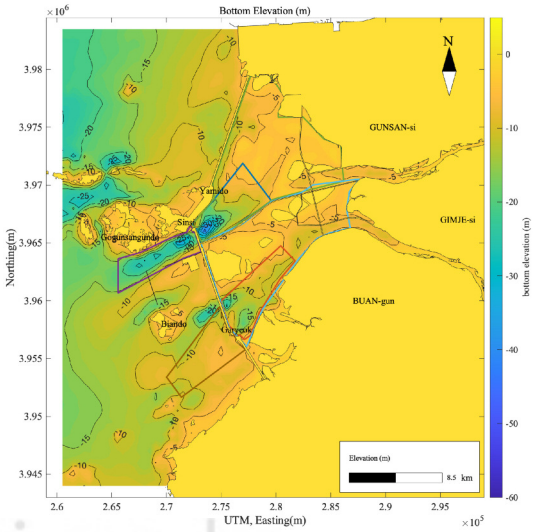

Figure 4. Six boxes for evaluating material transport characteristics

turbulent diffusion coefficients derived from EFDC's diffusion terms.

2. Definition of Analysis Boxes

To estimate the average concentration changes and total mass variations in each section, six boxes were defined as shown in Fig. 4. Box 1 corresponds to the inner area of the Sinsi sluice gate, Box 2 to the inner area of the Garyeok sluice gate, Box 3 to the outer area of the Garyeok sluice gate, Box 4 to the outer area of the Sinsi sluice gate, Box 5 to the Mangyeong region, and Box 6 to the Dongjin region. These boxes were consistently applied to all subsequent sectional analyses.

3. Evaluation of Vertical Salinity Gradient

Based on the average salinity values at the surface and bottom layers in each analysis box, the vertical salinity gradient was calculated to assess the degree of mixing and the presence of stratification within each region.

$$\Delta S = \overline{S_{surf}} - \overline{S_{bot}} \quad (1)$$

Here,

ΔS: Vertical salinity difference (psu)

$\overline{S_{surf}} - \overline{S_{bot}}$: Average salinity at the surface and bottom layers (psu)

4. Effective Diffusion Coefficient (Deff)

Deff is an index that comprehensively reflects physical effects in the ocean. In this study, both concentration-based (Eulerian) and particle-based (Lagrangian) effective diffusion coefficients were applied in parallel.

The concentration-based effective diffusion coefficient was derived from Fick's First Law and expressed as:

$$D_{eff} = \frac{J}{\partial C / \partial x} \quad (2)$$

Here,

J: substance flux per unit area (kg/m² · s)

$\frac{\partial C}{\partial x}$: spatial gradient of concentration

Since the particle-based effective diffusion coefficient cannot be defined using concentration fields, it was calculated using the mean square displacement proposed by Okubo (1971), which reflects the average degree of dispersion and spreading of particle clusters during the residence time:

$$D_{eff} = \frac{\langle (\Delta x)^2 + (\Delta y)^2 \rangle}{4t} \quad (3)$$

Here,

$\langle \cdot \rangle$: average over all particles in the box

Δx, Δy: displacement from the initial position

γ: residence time

III. Results and Discussion

1. Verification of tide and current

The data used for model validation consisted of tidal and current observations obtained from T-1, T-2, and PC-1, which were measured in January 2023, and from PC-2 (24LTC06), which was surveyed by the National Oceanographic Survey Agency in 2024 (Fig. 3). The tidal verification results showed that the relative mean absolute error ranged from 5.36% to 6.77%, and the index of agreement was high, ranging from 0.9144 to 0.9914 (Fig. 5). For current

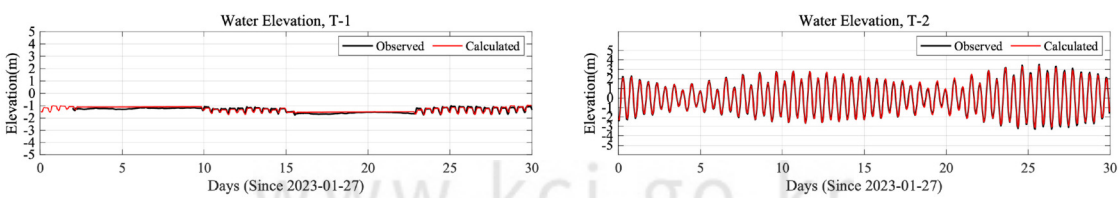

Figure 5. Tidal verification curve.

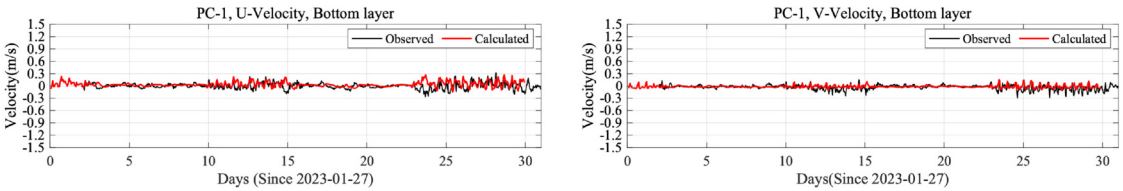

Figure 6. Velocity component verification curve at PC-1.

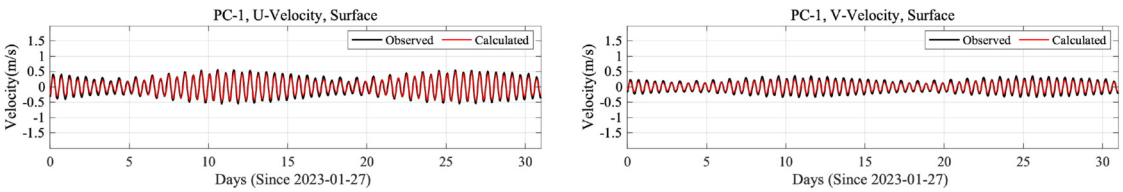

Figure 7. Velocity component verification curve at PC-2.

velocity verification, the relative mean absolute error was relatively small (10.01%–19.30%), and the cost function values were all less than 1, indicating "excellent" model performance (Fig. 6, 7). Therefore, the model successfully reproduced the observed water level, tide, and current conditions.

2. Flow and Residual Current Distribution

1) Flow reproduction

Fig. 8 presents the simulated flood and ebb currents during spring and neap tidal conditions. During the flood tide, the incoming tidal currents from the open sea entered the inner bay through the northern channel of Gaeya Island and the southern channel of Yubu Island, extending along the Gunsan coastline and reaching the front of the Geumgang Estuary Weir. In this process, the flow through the narrow channels was dominant, and the maximum current velocity exceeded approximately 1.5 m/s. During the ebb tide, the overall current velocity weakened, but the seaward outflow along the same narrow channels was still evident, with maximum velocities of about 1.4 m/s.

2) Changes Residual Flow Characteristics

Fig. 9 compares the distributions of surface and bottom residual currents before and after the construction of the

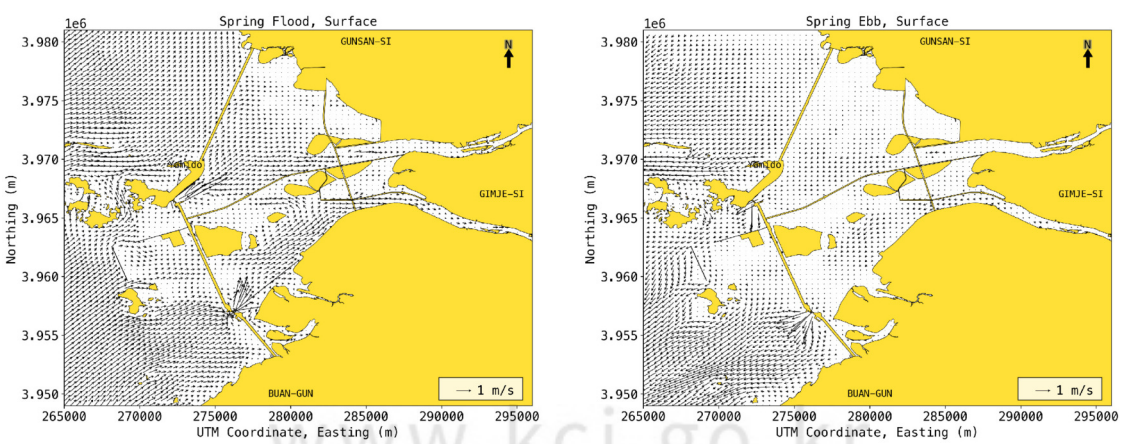

Figure 8. Surface current vectors at spring tide : (a) flood tide, (b) ebb tide

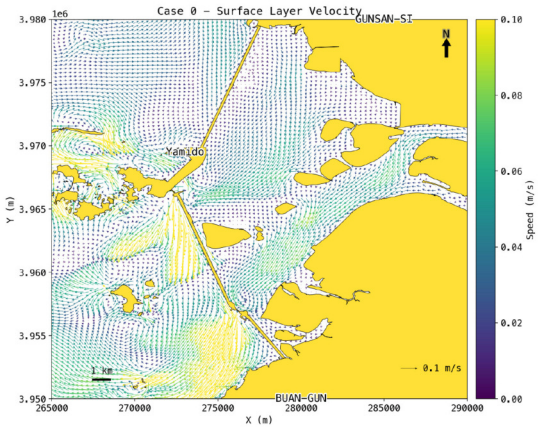

(a) surface

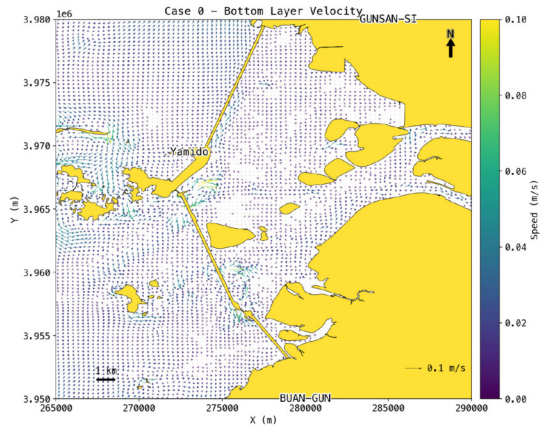

(b) bottom

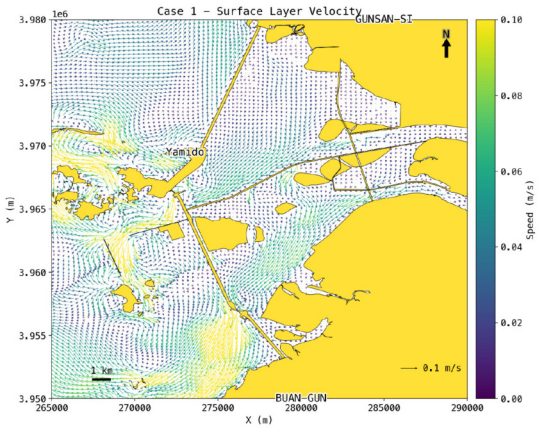

(c) surface

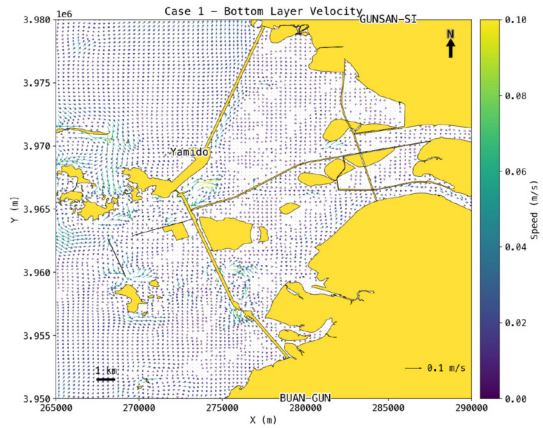

(d) bottom

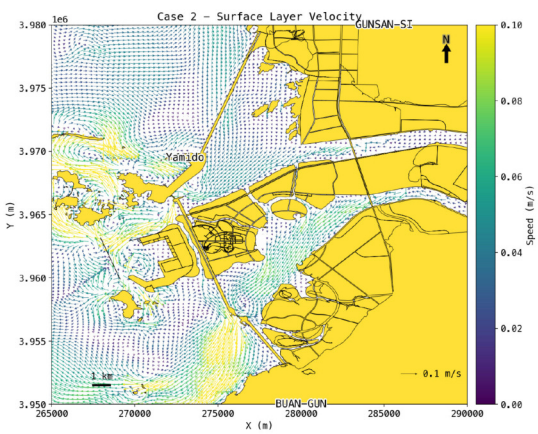

(e) surface

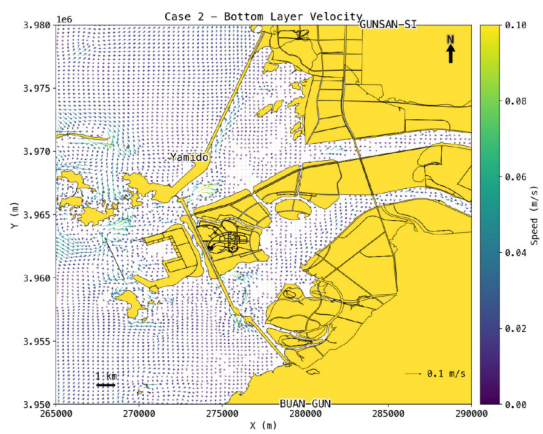

(f) bottom

Figure 9. Residual flow velocity for 30 days : (a), (b) case 0, (c), (d) case 1, (e), (f) case 2

Saemangeum New Port. At the surface, strong seaward flows induced by freshwater discharge were formed near the Sinsi and Garyeok sluice gates in all scenarios, but their primary directions and influence ranges exhibited clear variations depending on the development stage. In Case 0, the flow spread southward and southwestward; in Case 1, it shifted southwestward under the influence of the new port breakwater; and in Case 2, the southward flow was blocked by the outer breakwater, resulting in localized dispersion through the narrow channel.

At the bottom layer, a net inflow tendency opposite to the surface was dominant, which was consistently observed in both the inner and outer regions. In particular, high-salinity water continuously intruded in the direction opposite to the surface flow in front of the sluice gates. However, the flow velocity itself was weak, suggesting that its effect on material circulation was limited.

3. Salinity Structure Analysis

1) Salinity Distribution by Scenario

Fig. 10 illustrates the salinity variations in Cases 1 and 2 compared with Case 0 to evaluate material exchange efficiency during different construction phases. In Case 1, both surface and bottom salinity increased in the southern region of Saemangeum, reflecting enhanced

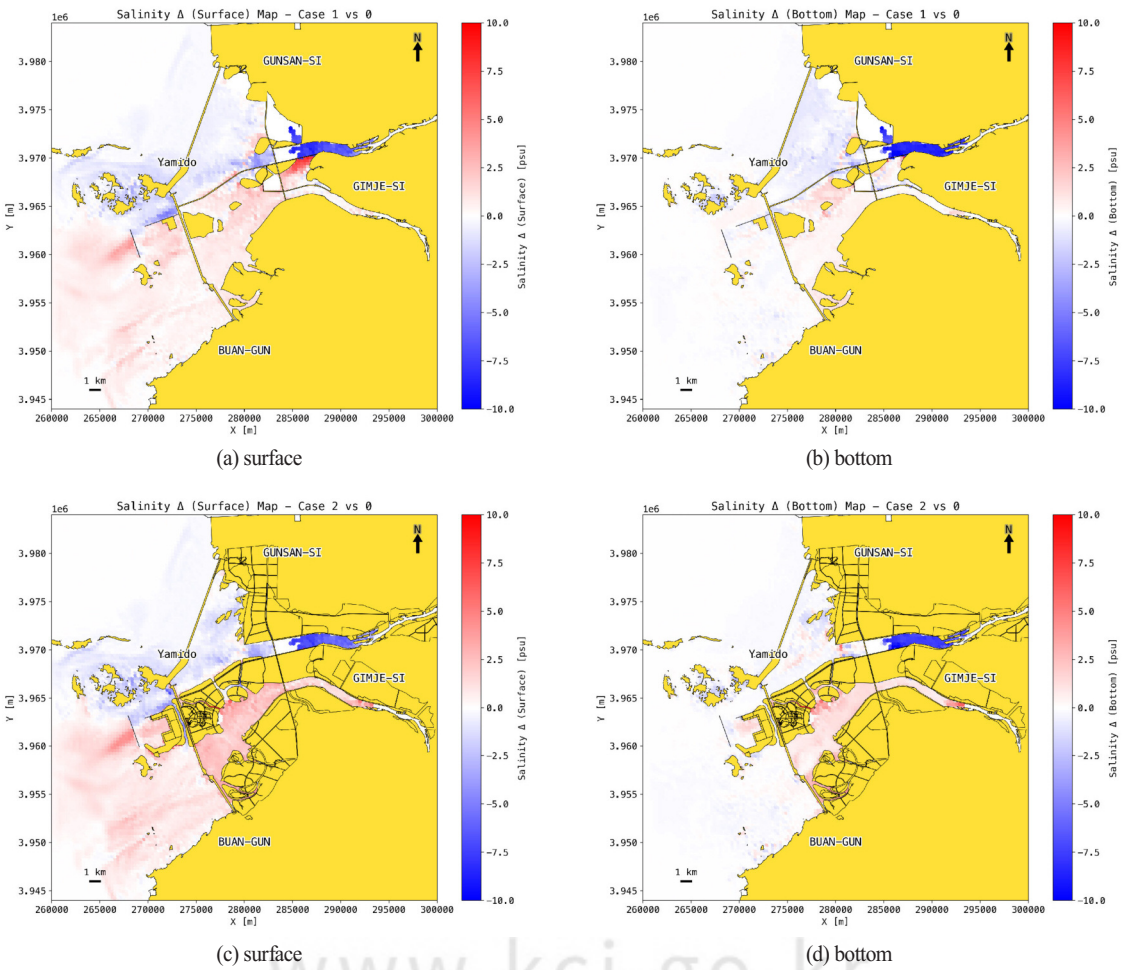

(a) surface (b) bottom

(c) surface (d) bottom

Figure 10. Changes in salinity concentration : (a), (b) case 1 and case 0, (c), (d) case 2 and case 0

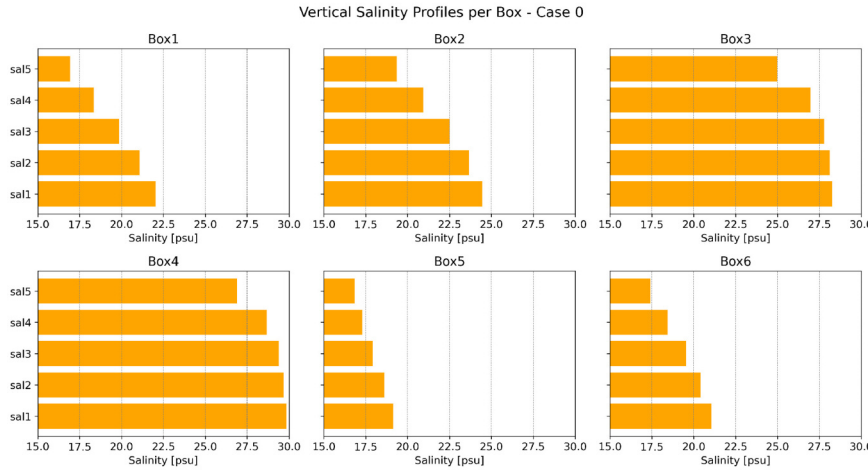

(a) Case 0

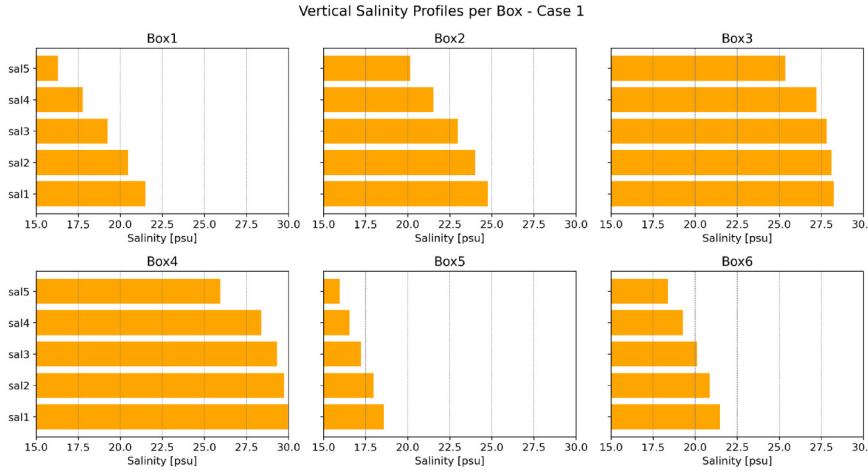

(b) Case 1

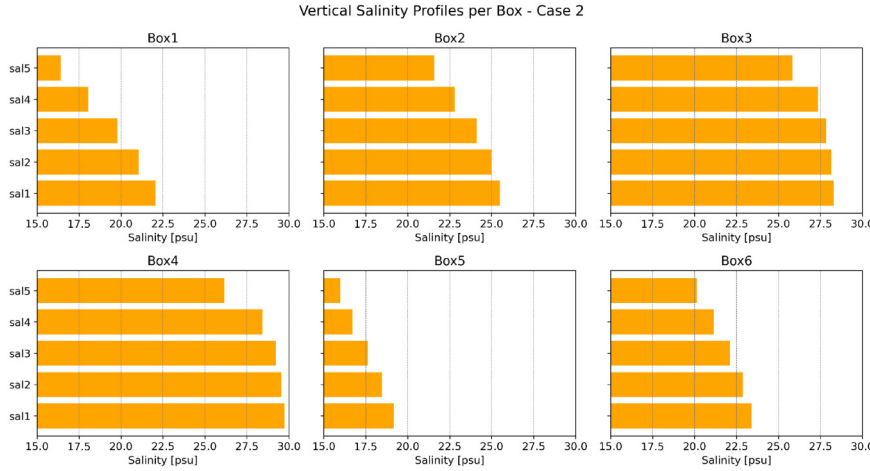

(c) Case 2

Figure 11. Vertical salinity profiles by box – Case 0, 1, 2

inflow through the Garyeok sluice following the east–west road construction. Conversely, the northern region showed a broad reduction in salinity, which can be attributed to increased freshwater inflow toward the western Saemangeum and the limited water exchange between the north and south. In Case 2, this contrast became more pronounced: northern salinity continued to decline, while the south exhibited a significant increase. The increase was especially large at the surface relative to the bottom, suggesting that vertical stratification would intensify as development progressed. These findings indicate that the hydrodynamic structure of Saemangeum is likely to evolve into a system with distinctly different characteristics between the northern and southern regions.

2) Vertical Salinity Gradient Analysis

To assess stratification and mixing, vertical salinity profiles from the surface (Sal5) to the bottom (Sal1) were analyzed (Fig. 11). In Case 0, strong stratification was observed in the inner regions (Boxes 1, 2, 5, and 6), while the outer regions (Boxes 3 and 4) showed relatively uniform salinity, indicating active vertical mixing. In Case 1, salinity increased in the southern regions (Boxes 2, 3, and 6), weakening the gradient, whereas the north (Boxes 1, 2, and 5) showed salinity reductions, with Box 4 exhibiting a strengthened gradient due to contrasting surface and bottom changes. This reflects enhanced exchange through the Garyeok sluice and weakened exchange at the Sinsi sluice. In Case 2, southern salinity rose further, reducing vertical gradients, while northern areas (Boxes 1 and 5) experienced intensified stratification due to bottom salinity increases. These results indicate more active exchange in the south but restricted inflow and worsening stagnation in the north.

4. Particle tracking experiments

Fig. 12 and 13 show the results of particle tracking experiments for the northern Mangyeong (Group 1) and

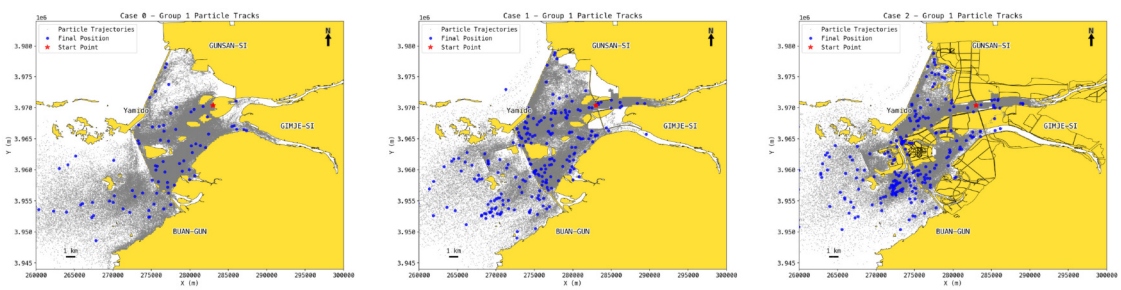

(a) Case 0 (b) Case 1 (c) Case 2

Figure 12. Particle trajectory and residual position by drop location – group 1

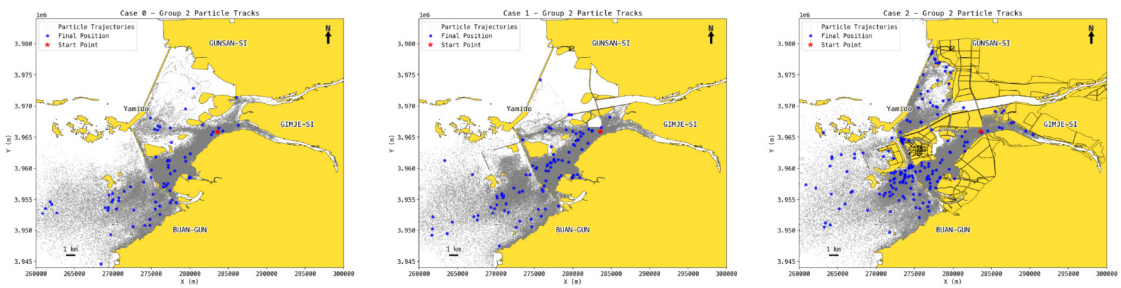

(a) Case 0 (b) Case 1 (c) Case 2

Figure 13. Particle trajectory and residual position by drop location – group 2

southern Dongjin regions (Group 2). In Case 0, particles from both groups dispersed irregularly across the interior and radiated seaward, with a tendency to concentrate in the south. In Case 1, the construction of the breakwater and east–west road restructured the pathways, strengthening seaward outflow near Sinsi Island (Group 1), while reducing southern dispersion (Group 2). In Case 2, particle movement in both regions became more aligned along the channels, enhancing connectivity between the Dongjin and Mangyeong regions. Overall, transport efficiency improved, but particle concentration in the narrow channels near the waterfront city indicated potential management vulnerabilities.

5. Deff diffusion change

1) Concentration-Based Deff

The concentration-based effective diffusion coefficient was derived from the mean salinity gradients of each analysis box to evaluate spatial variations in diffusion capacity under structural and topographic changes (Fig. 14). Boxes 3 and 4, located outside the sluice gates, consistently showed high values across all scenarios, remaining stable at 530 and 210 m^2/s in Case 2. By contrast, inner regions (Boxes 1, 5, and 6) exhibited declining values, with Boxes 5 and 6 decreasing from 160 and 99 m^2/s in Case 0 to 76 and 74 m^2/s in Case 2, reflecting weakened turbulence due to restricted flow pathways. Box 2 near the Garyeok sluice slightly increased, indicating enhanced connectivity with the open sea.

2) Particle-Based Deff

The particle-based effective diffusion coefficient represents the time-averaged spatial dispersion of individual particles and responds sensitively to channel structure and flow constraints. The analysis revealed spatially inconsistent variations across zones but a distinct contrast between the northern and southern sections (Fig. 15). In the

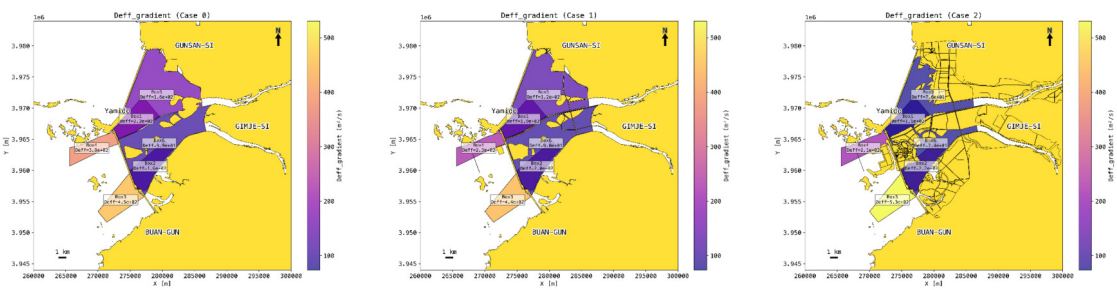

(a) Case 0 (b) Case 1 (c) Case 2

Figure 14. Concentration-based effective diffusion coefficient

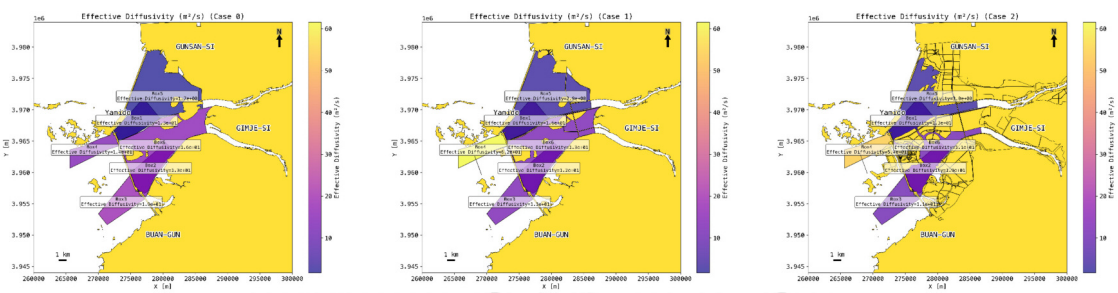

(a) Case 0 (b) Case 1 (c) Case 2

Figure 15. Particle-based effective diffusion coefficient

northern inner area of Saemangeum, variations in Box 1 were small and irregular across experimental cases. However, the diffusion coefficient in Box 5 increased slightly from 1.7 m^2/s in Case 0 to 3.0 m^2/s in Case 2, suggesting that channel reorganization increased the travel distance of particles. Conversely, the diffusion coefficient in Box 6, located on the southern side, decreased from 16 m^2/s in Case 0 to approximately 11 m^2/s in Case 2, indicating that structural installations reduced the diffusion capacity of the southern internal waterway. Meanwhile, Box 2 exhibited an increase of approximately 7.0 m^2/s in Case 2 compared to Case 1, reflecting enhanced connectivity between the inner and outer channels near the sluice gate.

The particle-based diffusion coefficient is a dynamic indicator statistically derived from the actual movement trajectories of individual particles, with its magnitude determined by particle displacement and residence time. In contrast, the concentration-based diffusion coefficient quantifies how spatial gradients of concentration (e.g., salinity) become homogenized over time, reflecting the average mixing effect at volumetric scales of several kilometers. Consequently, significant differences can occur between the two diffusion coefficients because they represent different physical scales and computational frameworks. The concentration-based diffusion coefficient reflects macroscopic mixing and dilution within the water body, whereas the particle-based diffusion coefficient characterizes the mobility and dispersion of individual particles; thus, the two indicators should be interpreted complementarily.

Specifically, in the Mangyeong water area (Box 5), the particle-based effective diffusion coefficient increased slightly from 1.7 m^2/s to 3.0 m^2/s, whereas the concentration-based effective diffusion coefficient markedly decreased from 160 m^2/s to 76 m^2/s. This result indicates that, although the average particle travel distance increased, the volumetric-scale diffusion range was actually reduced. Therefore, stagnation cannot be considered alleviated based solely on the particle-based diffusion coefficient. When the concurrent decrease in the concentration-based diffusion coefficient is considered, it suggests an increased risk of long-term retention and stagnation in the northern water area.

6. Comprehensive Interpretation of Stagnation Mechanisms

As development progressed, salinity appeared to decrease in the northern part of Saemangeum but increase in the southern part, giving the impression that stagnation was being alleviated. However, the salinity increase in the southern area was primarily attributed to a reduction in the volume of the Dongjin water area due to internal reclamation, as well as enhanced connectivity with the open sea through the sluice gates. These findings suggest that after Saemangeum's completion, seawater exchange will become more active in the southern Dongjin area, whereas inflow restriction in the northern Mangyeong area may intensify stagnation.

Furthermore, a comparison of spatial diffusion characteristics based on the concentration-based and particle-based effective diffusion coefficients revealed that the concentration-based coefficient generally decreased in Case 2. This result indicates that although substantial concentration gradients remained, diffusion flux diminished as material exchange became restricted after development, leading to a reduced effective diffusion coefficient. In other words, concentration differences persisted, but the physical mixing capacity to mitigate them weakened. Conversely, the particle-based effective diffusion coefficient indicated that the transport distance was maintained or slightly increased due to straighter flow paths; however, physical constraints narrowing the overall diffusion range also emerged, implying that stagnation actually intensified.

IV. Conclusion

This study quantitatively investigated the characteristics

of seawater inflow and material dispersion resulting from the Saemangeum development using a numerical model and the effective diffusion coefficient (Deff) as a diagnostic indicator. The analysis results revealed contrasting regional responses: seawater exchange was enhanced in the southern Dongjin area after development, whereas the northern Mangyeong area exhibited intensified stagnation due to circulation blockage and reduced mixing. Furthermore, the concentration-based Deff indicated that although concentration gradients were maintained, the overall mixing capacity weakened, while the particle-based Deff reflected a reduced diffusion range caused by channel constraints. The combined interpretation of both indicators demonstrated that structural installations restricted material exchange and reinforced stagnation. This intensified stagnation extends beyond simple hydrodynamic changes and may directly affect the urban and port functions of the Saemangeum area after development. Particularly in the Mangyeong area, prolonged stagnation increases the risk of dissolved oxygen (DO) depletion, eutrophication, and odor generation, thereby reducing recreational and environmental value. Sediment accumulation and water quality deterioration could also increase the maintenance burden of port operations. Therefore, effective water quality management in Saemangeum requires an integrated strategy that considers the spatial distribution of stagnation zones and channel structural changes, rather than relying solely on flow velocity–based indicators.

Meanwhile, since the numerical simulations were conducted under winter conditions, the results have seasonal limitations. Winter is a period dominated by full-depth mixing, whereas stagnation phenomena are expected to intensify during summer when thermal stratification develops. Therefore, future research should perform seasonal comparative simulations, including the stratification period (summer), to comprehensively assess material exchange characteristics over extended time scales.

References

전진석. (2003). 새만금 간척사업의 정치경제와 정책옹호연합모형. 한국사회와 행정연구, 14 (2), 207-234.

Chun, J. (2003). Political economy of Saemangeum Tideland reclamation project through advocacy coalition framework. *Korean Society and Public Administration, 14*(2), 207-234.

Fick, A. (1855). V. On liquid diffusion. *Philosophical Magazine, 10*(63), 30-39. https://doi.org/10.1080/14786445508641925

정희영, 류인구, 정세웅. (2009). EFDC 모형을 이용한 새만금호 내 해수유통량에 따른 오염물질 혼합변화 모의, 한국농공학회논문집, 51(6), 53-62.

Jeong, H. Y., Ryu, I. G., & Chung, S. W. (2009). Simulations of pollutant mixing regimesin seamangeum lake according to seawater exchange rates using the EFDC model. *Journal of the Korean Society of AgriculturalEngineers, 51*(6), 53-62.

김종구, 김양수. (2002). 새만금 사업지구의 연안해역에서 부영양화관리를 위한 생태계모델의 적용 - 1. 해역의 수질 특성 및 저질의 용출 부하량 산정. 한국수산과학회지, 35(4), 348-355.

Kim, J. G.,& Kim, Y. S. (2002). Application of Ecosystem Model for Eutrophication Control. *Journal of Korean Fish. Society, 35*(4), 348-355.

고재원, 조홍연, 정신택, 권혁민. (2002). 만경강·동진강 유역의 오염물질 유출모델링, 한국해안·해양공학회논문집. 14 (2), 108-115.

Ko, J. W., Cho, H. Y., Jeong, S. T., & Kweon, H. M. (2002). Pollutants discharge modeling in Mankyung and Dongjin Rivers. *Journal of Korean Society of Coastal and OceanEngineers, 14*(2), 108-115.

이성호. (2008). 새만금 간척사업과 지역 성장정치. 지역사회연구, 16(4), 55-77.

Lee, S. H. (2008). Saemangeum reclamation project and local growth politics: focusing on counter move of local growth coalition. *Journalof Regional Studies,*

16(4), 55-77.

Okubo, A. (1971). Oceanic diffusion diagrams. *In Deepsea Research and Oceanographic Abstracts, 18*(8), 789-802. https://doi.org/10.1016/0011-7471(71)90046-5

박종대. (2016). 새만금사업단 소개. 물과 미래, 49(11), 97-102

Park, J. D. (2016, November). Introduction of the Saemangeum Project. *Waterfor Future, 49*(11), 97-102. Korea Rural Community Corporation.

박성화, 김종구, 권민선. (2023). 새만금 배수갑문 운영에 따른 염분 변화와 저층수의 입자교환 모의. 해양환경안전학회지, 29 (6), 562-575.

Park, S., Kim, J., & Kwon, M. (2023). Salinity Changes and Bottom Water Particle Exchange Simulations in Response to Sluice Gate Operations at Saemangeum Lake. *Journal of the Korean Society of Marine Environment & Safety, 29*(6), 562-575.

서승원, 조완희. (2007). 새만금호 완공전후의 수동역학변화 해석. 대한토목학회논문집 B, 27(3B), 361-369.

Suh, S. W., & Cho, W. H. (2007). Hydraulic change analysis on Saemangeum reservoir after final closure. *Journal of the Korean Society of Civil Engineers, 27*, 361-369.

서승원, 이화영. (2011). 입자추적방법을 이용한 새만금 해역의 수리특성 변화 분석. 한국해안·해양공학회논문집, 23(6), 442-450.

Suh, S. W., & Lee, H. Y. (2011). Analysis of hydrodynamic change around the Saemangeum area using a particle tracking method. *Journalof Korean Society of Coastal and Ocean Engineers, 23*(6), 442-450.

전라북도. (2017). 새만금호 내부 수질 특성 및 관리방안 연구용역 보고서.

Jeollabuk-do. (2017). Final report on the study for water quality characteristics and management strategies of the Saemangeum Lake.

정석일, 유형주, 류광현, 이승오. (2018). 새만금 종합개발계획에 따른 새만금 유역 치수 안전성 수치모의. 한국안전학회지, 33(5), 127-133.

Jeong, S. I., Yoo, H. J, Ryu, K. H., & Lee, S. O. (2018). Numerical Simulation for River Safety of Saemangeum Basin according to Master Plan. *Journal of the Korean Society of Safety, 33*(5), 127-133

유상철, 서승원, 이화영. (2012). 새만금 내부개발이 체류시간 및 수질변화에 미치는 영향. 한국해양환경·에너지학회지, 15(3), 186-197.

Yoo, S. C., Suh, S. W., & Lee, H. Y. (2012). Impacts on residence time and water quality of the Saemangeum reservoir caused by inner development. *Journal of the Korean Society for Marine Environment & Energy, 15*(3), 186-197.